Chinese Chemical Letters 34 (2023) 107490

Contents lists available at ScienceDirect

Chinese Chemical Letters

journal homepage: www.elsevier.com/locate/cclet

Fully conversing and highly selective oxidation of benzene to phenol based on MOFs-derived CuO@CN photocatalyst

Longjiang Sun[a,b], Dongxu Wang[a], Yuxin Li[a,*], Baogang Wu[a], Qi Li[a], Cheng Wang[a,d,*], Shuao Wang[c], Baojiang Jiang[a,*]

[a] Key Laboratory of Functional Inorganic Material Chemistry, Ministry of Education of the People's Republic of China, School of Chemistry and Materials Science, Heilongjiang University, Harbin 150080, China
[b] School of Pharmacy, Jiamusi University, Jiamusi 154007, China
[c] State Key Laboratory of Radiation Medicine and Protection School for Radiological and interdisciplinary Sciences (RAD-X) and Collaborative Innovation Center of Radiation Medicine of Jiangsu Higher Education Institutions, Soochow University, Suzhou 215123, China
[d] Guangdong Laboratory of Chemitry and Fine Chemical Industry Jieyang Center, Guangdong University of Technology, Jieyang 510006, China

ARTICLE INFO

Article history:
Received 13 March 2022
Revised 2 April 2022
Accepted 4 May 2022
Available online 10 May 2022

Keywords:
Photocatalysis
MOF
CuO@CN
Selectivity oxidation
Highly conversion rate

ABSTRACT

Developing highly efficient photocatalysts for selective oxidation of benzene to phenol is of great significance. However, it is still challenging to simultaneously achieve high conversion rate and selectivity. Herein, we demonstrate 99.9% of benzene photoconversion and 99.1% of phenol selectivity under the illumination of AM 1.5 for 12 h. For this purpose, an advanced CuO@CN photocatalyst has been fabricated by loading tubular carbon nitride (CN) with CuO nanoparticles thermally polymerized from Cu-based metal-organic frameworks (MOFs). The sluggish photocharge carrier recombination rate and the excellent stability indicate that the as-prepared nanocomposite is an ideal photocatalyst for benzene oxidation application. This work paves a new avenue for designing novel photocatalyst based on MOFs and carbon nitride materials.

Phenol, one of common-used industrial chemicals, is widely applied in the manufacture of pharmaceutical compounds, phenolic resins, dyes and plastics [1–3]. However, conventional three-step cumene production process in current industry suffers from high energy consumption, low conversion rate and large quantities of by-products [4]. Therefore, it is imperative to develop a novel strategy to solve the above shortcomings. Recently, one-step process as an attractive route in phenol production has been developed for the straight and selective oxidation of benzene to phenol, with the aid of environmentally friendly oxidants such as N_2O, O_2 and H_2O_2 [5–10]. Among them, H_2O_2 is commonly considered as a promising oxidant because of its advantages on low cost and environment friendly process with H_2O as the only by-product. However, direct utilization of H_2O_2 as an oxidant often yields unsatisfied benzene-to-phenol efficiency, mainly due to the lack of suitable platforms to enrich hydrogen peroxide and benzene and further promote the oxidizing reaction.

Based on this, much progress has been made to develop co-catalysts for improving the benzene-to-phenol activity and selectivity with H_2O_2 as oxidant, such as Fe-based MOFs (MIL-101, 30.6% conversion rate) [11], Fe-doped and Cu-grafted ordered silica SBA-15 composite (Cu/Fe-SBA-15, 35.5% conversion rate and 89.8% selectivity) [12], copper single-atom catalyst (Cu-SA/HCNS, 86.0% conversion rate and 96.7% selectivity) [13]. However, there is no catalyst capable of achieving complete conversion of benzene and single selectivity of phenol, despite the importance of these indicators in industrial production.

Because of its structural diversity and adjustability, metal-organic frameworks (MOFs) can be used as a very promising photocatalyst, which have been widely used in water splitting, CO_2 reduction, degradation of pollutants, and selective oxidation of organics [14–17]. Herein, a novel photocatalyst, CuO@CN composite, has been prepared by high-temperature calcination of precursor synthesizing by *in situ* loading Cu-based MOFs onto the surface of tubular carbon nitride (TCN) under solvothermal method. The CuO@CN composite material as the catalyst possesses the follow advantages: (1) Metal with the high conductivity is the optimal candidate to modify CN, which can effectively promote the charge separation and transfer for CN. (2) CuO nanoparticles are uniformly loaded on the surface of CN, which is conductive to increase the

* Corresponding authors at: Key Laboratory of Functional Inorganic Material Chemistry, Ministry of Education of the People's Republic of China, School of Chemistry and Materials Science, Heilongjiang University, Harbin 150080, China.
E-mail addresses: liyuxin@hlju.edu.cn (Y. Li), wangc_93@163.com (C. Wang), jbj@hlju.edu.cn (B. Jiang).

https://doi.org/10.1016/j.cclet.2022.05.004
1001-8417/

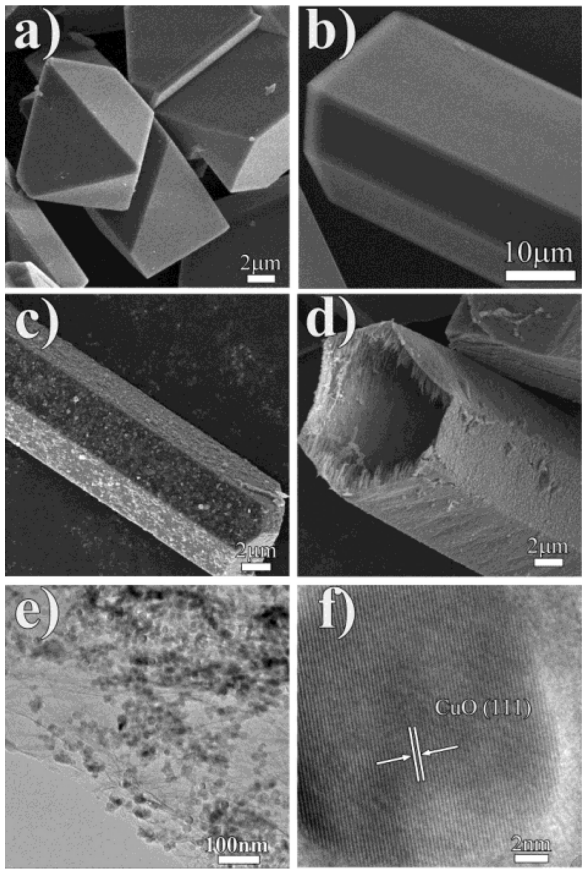

Fig. 1. (a–c) SEM photographs of MOF, TCN and MOFs/TCN. (d) SEM photographs of CuO@CN. (e) TEM photographs of CuO@CN. (f) HRTEM photographs of CuO@CN.

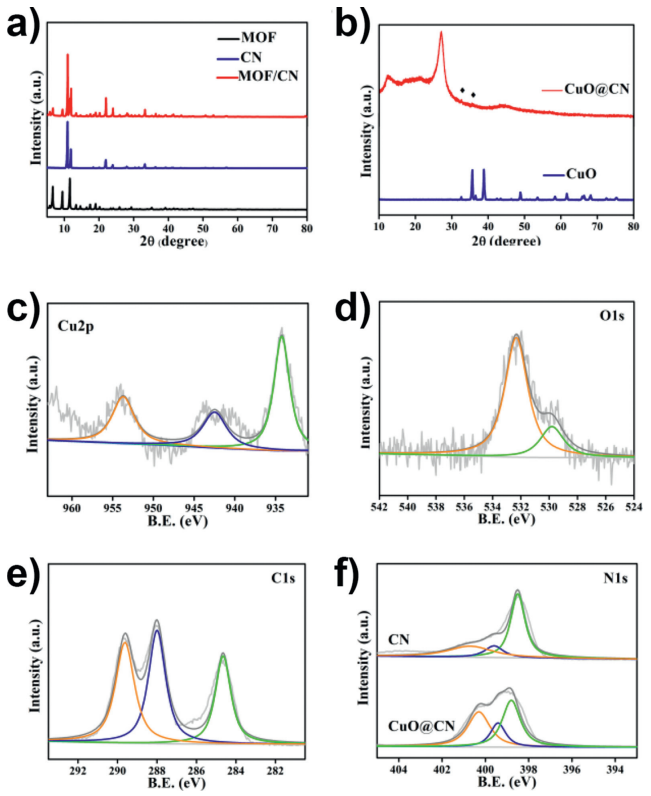

Fig. 2. (a) XRD patterns of the synthesized MOFs, TCN and MOFs/TCN. (b) XRD patterns of the synthesized CuO and CuO@CN. XPS spectra of CuO@CN: (c) Cu 2p, (d) O 1s, (e) C 1s and (f) N 1s.

interfacial contact area and further to enhance the catalytic efficiency. (3) The heterojunction structure of CuO and CN can effectively inhibit the recombination of charge carriers and improve the utilization efficiency of charge carriers [18], thus greatly improving the catalytic activity of the CuO@CN composites. Benefiting from these above advantages, the CuO@CN composite photocatalyst is expected to exhibit excellent catalytic performance in selective oxidation of benzene to phenol, being of a great potential for practical application. This work paves a new avenue for designing and preparing effectively catalyst based on MOFs materials and CN [19–21].

Firstly, the characterization analyses are carried out to as-prepared composites. According to the scanning electron microscopy (SEM) images (Fig. 1a), the Cu-MOFs features a regular octahedral geometry which consistent with previous reports [22–24]. The supramolecular precursor for TCN has a hexagonal structure with a radius of 30 μm (Fig. 1b). After uniformly loading the Cu-MOFs onto the surface of the TCN rod, the size of the Cu-MOFs is obvious decreased (Fig. 1c). In addition, we synthesized MOFs/TCN loaded with different contents of MOFs. It can be seen from the SEM (Fig. S2 in Supporting information), when the amount of $Cu(OAC)_2{\cdot}3H_2O$ and H_3BTC increases, the surface of TCN is modified with more MOFs with more small size. After thermal calcination, the obtained CuO@CN exhibits the hollow tubular morphology with uniform filamentous structure in inner surface and solid particles loaded on the outer surface (Fig. 1d). For clarity, magnified images have been collected and show more clearly structural features (Fig. S3 in Supporting information). To further confirm the structure and morphology, transmission electron microscopy (TEM) images of the CuO@CN sample have been carried out. As displayed in Fig. 1e, CuO nanoparticles are uniformly loaded on the surface of CN, and the morphology of Cu-MOFs is well maintained. We can observe that the average particle size of CuO is approximate 15 nm (Fig. S4 in Supporting information). In the high-resolution transmission electron microscopy (HRTEM) of CuO@CN, there is a clear observation of the lattice fringe of 0.232 nm that matches well with the (111) plane of CuO (Fig. 1f). This indicates that CuO nanoparticles have been successfully supported on the surface of CN. The corresponding elemental mappings of CuO@CN composite materials are also delineated. As expected, C, O, Cu and N atoms are equally dispersived in the photocatalyst (Fig. S5 in Supporting information), which further prove the successful loading of CuO on the CN.

Powder X-ray diffraction (PXRD) patterns further certify the above analysis. The PXRD patterns of CuO@CN reveal the simultaneous presence of the CN and CuO nanoparticles (Figs. 2a and b). The peaks located at 2θ values of 32.5° and 35.5° can be indexed to the (110) and $(11\bar{1})$ facets of CuO, respectively. The low intensity of the diffraction peak of CuO results from the low content of the loaded CuO. Meanwhile, Fourier transmission infrared (FT-IR) spectra (Fig. S1 in Supporting information) are traced to obtain further structural information on the as-synthesized catalysts. The broad peak at 2900∼3200 cm^{-1} attributes to the N-H and O-H bands, due to the presence of residual amino groups and absorbed H_2O molecules, respectively. The absorption band ranging from 1200 cm^{-1} to 1600 cm^{-1} is the characteristic vibration signal of the aromatic CN heterocycles [25], indicating that loading CuO nanoparticles did not change the structure of CN.

To probe the elemental composition and the oxidation state, the systematic analysis on X-ray photoelectron spectroscopy (XPS) of CuO@CN has been subsequently performed. As displayed in Fig. 2c, the Cu 2p spectrum in CuO@CN consists of three peaks located at

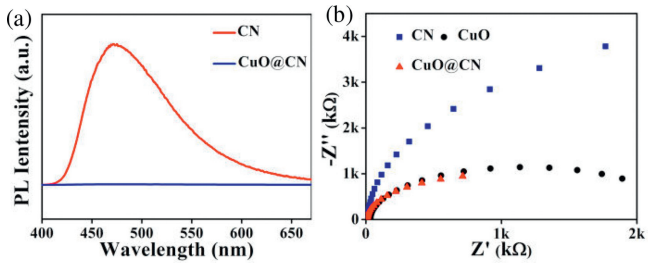

Fig. 3. (a) Steady-state PL spectra of CN and CuO@CN. (b) Nyquist plots of CN, CuO and CuO@CN.

934.2 eV and 953.7 eV, attributing to Cu $2p_{3/2}$ and Cu $2p_{1/2}$ of CuO, respectively. The peak at 941.9 eV belongs to Cu $2p_{3/2}$ satellite peak of CuO. These results reveal that CuO is successfully loaded onto the CN surface, consistent with the XRD and TEM results. In Fig. 2d, the high-resolution XPS spectrum of O 1s spectrum is deconvoluted into two main peaks at 530.7 eV and 532.4 eV, which are assigned to Cu-O and C-O bond, respectively. For C 1s spectrum, three main peaks located at 284.65, 288.0 and 289.6 eV have been deconvoluted and assigned to C-C, C-N and C-O bond, respectively (Fig. 2e). The high-resolution XPS spectrum of O 1s and C 1s of pure CN are shown in Figs. S6 and S7 (Supporting information). Fig. 2f shows that N 1s spectrum of CN has three peaks at 398.5, 399.6 and 400.7 eV, which are allocated to the C-N=C, N-$(C)_3$ and C-N-H bonds. The N 1s spectrum of the CuO@CN shows three pinnacles of C-N=C, N-$(C)_3$ and C-N-H bonds located at 398.9, 399.5 and 400.3 eV, respectively. It is noticeable that the C-N=C peak of CuO@CN moves towards higher binding energy but C-N-H peak moves towards lower binding energy in comparison to them of CN. These results demonstrate the strong mutual interaction and electronic transfer between CuO and CN, which is beneficial to improve the catalytic activity of composites.

In the process of photocatalysis, it is significant influence factor that the separation of electron-hole pairs and their rapid migration toward the active center of the catalysts [26–28]. As displayed in Fig. 3a, the photoluminescence (PL) intensity of CuO@CN decreases significantly in comparison with that of CN, which should be evaluated to the rapid transfer of photogenerated electrons from CN to CuO and thus suppressing the recombination of electron-hole pairs, which greatly improves the utilization rate of photogenerated electrons and thus improves the catalytic activity of the catalyst. In the Nyquist plots (Fig. 3b), the diameter of the semicircle for CuO@CN is smaller than those for CN and CuO, suggesting that the CuO@CN composite has the most efficient charge transfer. In other words, CuO nanoparticles anchored on CN can effectively increase visible-light harvesting and promote the separation and transfer of photo-induced electron-hole pairs [29,30].

Subsequently, the catalytic performance of CuO@CN composite is evaluated by employing selective oxidation of benzene to phenol in one-step process. Without the CuO@CN catalyst, little benzene is converted under the illumination of AM 1.5 for 12 h (Table S1 in Supporting information, entry 1). For the CN as photocatalyst, the conversion rate and the selectivity increase to 8.5% and 94.4%, respectively (Table S1, entry 2). Remarkably, CuO@CN composite exhibits obviously improving photocatalytic performance. Concurrently, CuO nanoparticles anchored on CN can effectively promote the separation and transfer of photo-induced electron-hole pairs. The above results show that CuO and CN have a good synergistic effect. When the reaction was conducted under the illumination of AM 1.5 for 12 h, the conversion and selectivity were increased to 99.9% and 99.1%, respectively, which are significantly higher than those of CN (Fig. 4a and Table S1). Even though in the absence of visible light, the CuO@CN catalyst shows 16.4% of benzene conversion with 98.0% of phenol selectivity in the dark and 63.7% of benzene conversion with 93.1% of phenol selectivity at 80 °C for 12 h. The state-of-the-art benzene conversion rate and phenol selectivity indicate that the as-prepared CuO@CN composite is an ideal benzene-to-phenol photocatalyst which is of practical values in industry.

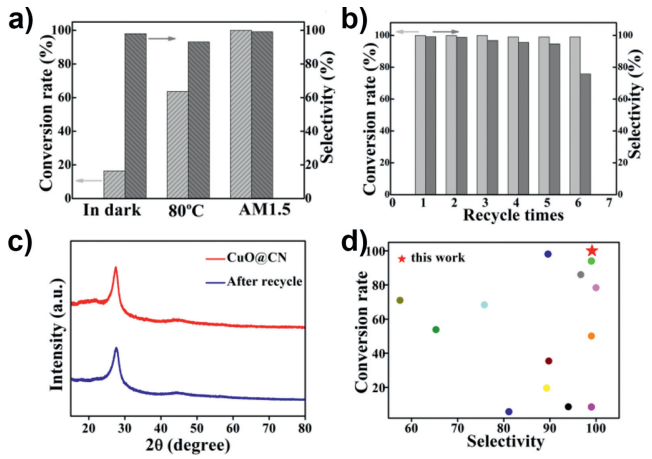

Fig. 4. (a) Conversion rate and selectivity of CuO@CN at different conditions. (b) The recycle performance of CuO@CN. (c) XRD patterns of CuO@CN and after recycle. (d) Comparison of catalytic activity of CuO@CN with previously reported catalysts for selective oxidation of benzene to phenol [11–13,31–40].

Table 1
Selective oxidation of benzene to phenol.

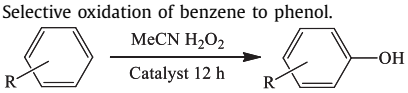

Entry	Reactant	Product	Conversion (%)	Selectivity (%)
1			99.9	99.1
2		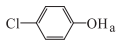	99.0	99.0
3		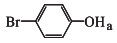	99.0	99.0
4		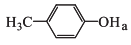	97.9	98.6
5		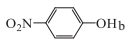	90.5	99.0

Reaction conditions: Reactant (1 mmol), 30% H_2O_2 (6 mL), MeCN (6 mL), cat. (40 mg), 12 h and AM 1.5 illumination. Conversion and selectivity demined by GC-Ms.
[a] *Ortho*- and *para*-substituted phenols as the main products.
[b] *Ortho*-, *meta*- and *para*-substituted phenols as the main products.

In addition to the remarkable catalytic properties, the high stability of CuO@CN composite is an outstanding advantage for industrial application. Fig. 4b shows that even after five cycles, the conversion rate of benzene and selectivity of phenol still remain high levels, with indiscernible decline in benzene conversion rate and phenol selectivity. After five cycles of reaction, the results of ICP analysis show that the content of copper did not decrease significantly from 1.18% to 0.90% (Table S2 in Supporting information). These results strongly show that CuO@CN composite is a very active and stable catalyst for the oxidation of benzene to phenol. Additionally, the PXRD pattern of CuO@CN photocatalyst shows the unchanged structure after five cycles (Fig. 4c). This further proves that CuO@CN is a promising catalyst for the oxidation of benzene to phenol (Fig. 4d and Table S3 in Supporting information). Furthermore, the application scope of this catalytic system is explored by using a variety of benzene derivatives contain electron-withdrawing or electron-donating substituents under the same reaction conditions. As summarized in Table 1, the CuO@CN compos-

ite also exhibits good activity for oxidation of benzene derivatives. When using chlorobenzene and bromobenzene as the substrate, both the conversion rate of benzene and the selectivity of phenol reach up to 99.0% (Table 1, entries 2 and 3). The main products are *ortho*- and *para*-substituted phenol. A similar effect is observed on methylbenzene (Table 1, entry 4). When using nitrobenzene with electron-withdrawing substituents as the substrate, there is a little decrease on the conversion rate of benzene (90.5%) with *ortho*-, *meta*- and *para*-substituted phenol as the main products (Table 1, entry 5). The above results indicate that CuO@CN catalyst have good catalytic activity and functional group tolerance for the oxidation of benzene to phenol containing different electron-withdrawing or electron-donating substituents.

Then, 5,5-dimethyl-1-pyrroline-*N*-oxide (DMPO) is used as hydroxyl radical trapping agent [41]. Fig. S8 (Supporting information) shows an EPR spectrum observed during the reaction of benzene with H_2O_2 in the presence of CuO@CN and DMPO under the illumination of AM 1.5 and in the dark. The results show four typical signals for the DMPO-$^{\bullet}$OH adduct under AM 1.5 illumination, which confirms the formation of $^{\bullet}$OH radicals during the photocatalytic reaction. This shows that selective oxidation of benzene to phenol over CuO@CN follows a $^{\bullet}$OH radicals mediated oxygenation pathway. Therefore, CuO@CN catalyst has the superior electron trapping ability and can effectively inhibit the recombination of electrons and holes, which is the significant reason to interpret the excellent photocatalytic activity of CuO@CN. Based on the above analysis, the mechanism for photocatalytic selective oxidation of benzene to phenol over CuO@CN has been proposed. First, efficient excitation of CuO@CN by the illumination of AM 1.5 takes place and the photoresponse simultaneously forms electron and hole charge carriers. Then, the photogenerated electrons can react with H_2O_2 to form $^{\bullet}$OH radicals. The last step, the photogenerated $^{\bullet}$OH takes part in the selective oxidation of benzene to phenol. Meanwhile, the holes can directly react with benzene to form phenol [34,39]. The possible mechanism diagram for photocatalytic selective oxidation of benzene to phenol over CuO@CN is shown in Scheme S1 (Supporting information). Thus, CuO@CN shows a superior performance for the selective oxidation of benzene to phenol.

In summary, a CuO@CN composite with uniform dispersion of CuO nanoparticles on the surface of CN has been successfully designed and fabricated by the high temperature calcination of Cu-MOFs/TCN precursor. CuO nanoparticles tightly contact with CN, which promotes the transfer of photogenerated electrons from CN to CuO, effectively inhibits the recombination of electrons and holes, as well as shows excellent catalytic activity in the selective oxidation of benzene to phenol. Remarkable, the benzene conversion rate and phenol selectivity achieve 99.9% and 99.1%, respectively, suggesting a great potential for practical application. Our powerful results show that Cu-MOFs/TCN-derived CuO@CN materials would endow them with better change to be applied in more areas of catalysis.

Declaration of competing interest

We declare that we have no financial and personal relationships with other people or organizations that can inappropriately influence our work.

Acknowledgments

This work was supported by National Natural Science Foundation of China (Nos. 21771061, U2001219, 52103225, 51973051 and 81961138010) and the Outstanding Youth Fund of Heilongjiang Province (No. JQ 2020B002), National Key R&D Program of China (No. SQ2021YFE012298).

Supplementary materials

Supplementary material associated with this article can be found, in the online version, at doi:10.1016/j.cclet.2022.05.004.

References

[1] P. Borah, X. Ma, K.T. Nguyen, Y. Zhao, Angew. Chem. Int. Ed. 51 (2012) 7756–7761.
[2] S. Fukuzumi, K. Ohkubo, Asian J. Org. Chem. 4 (2015) 836–845.
[3] T. Tsuji, A.A. Zaoputra, Y. Hitomi, et al., Angew. Chem. Int. Ed. 56 (2017) 7779–7782.
[4] S.S. Niwa, M. Eswaramoorthy, J. Nair, et al., Science 295 (2002) 105–107.
[5] M.L. Bols, H.M. Rhoda, B.E.R. Snyder, et al., Dalton Trans. 49 (2020) 14749–14757.
[6] C. Ouyang, Y. Li, J. Li, Catalysts 9 (2019) 44.
[7] Y.Y. Gu, X.H. Zhao, G.R. Zhang, H.M. Ding, Y.K. Shan, Appl. Catal. A: Gen. 328 (2007) 150–155.
[8] W. Wang, G. Ding, T. Jiang, et al., Green Chem. 15 (2013) 1150–1154.
[9] D. Wei, L. Huang, H. Liang, et al., Catal. Sci. Technol. 11 (2021) 5931–5937.
[10] P. Basyach, A.K. Guha, S. Borthakur, et al., J. Mater. Chem. A 8 (2020) 12774–12789.
[11] D. Wang, M. Wang, Z. Li, ACS Catal. 5 (2015) 6852–6857.
[12] Y. Wu, X. Zhang, F. Wang, et al., Ind. Eng. Chem. Res. 60 (2021) 8386–8395.
[13] T. Zhang, D. Zhang, X. Han, et al., J. Am. Chem. Soc. 140 (2018) 16936–16940.
[14] Y. Liu, H. Cheng, M. Cheng, et al., Chem. Eng. J. 417 (2021) 127914.
[15] Y. Liu, C.S. Tang, M. Cheng, et al., ACS Catal. 11 (2021) 13374–13396.
[16] H.D. Liu, M. Cheng, Y. Liu, et al., Coord. Chem. Rev. 458 (2022) 214428.
[17] W. Zhang, Y. Tian, H. He, et al., Nat. Sci. Rev. 7 (2020) 1702–1725.
[18] Y. Chen, J.F. Li, P.Y. Liao, et al., Chin. Chem. Lett. 31 (2020) 1516–1519.
[19] Q. Li, S.X. Li, J.Q. Sha, et al., ACS Appl. Nano Mater. 4 (2021) 12197–12203.
[20] C.C. Wang, X.H. Yi, P. Wang, Appl. Catal. B: Environ. 247 (2019) 24–48.
[21] A. Bavykina, N. Kolobov, I.S. Khan, et al., Chem. Rev. 120 (2020) 8468–8535.
[22] M.K. Albolkany, W. Y, W.J. Li, et al., Angew. Chem. Int. Ed. 59 (2020) 21499–21504.
[23] T. Wei, M. Zhang, P. Wu, et al., Nano Energy 34 (2017) 205–214.
[24] N. Bhoria, G. Basina, J. Pokhrel, et al., J. Hazard. Mater. 394 (2020) 122565.
[25] X.D. Xiao, Y. Gao, L. Zhang, et al., Adv. Mater. (2020) e2003082.
[26] Y. Chen, Z. Zhan, J. Wang, et al., Chin. Chem. Lett. 29 (2018) 437–440.
[27] B.G. Wu, L. Zhang, B.J. Jiang, et al., Angew. Chem. Int. Ed. 60 (2021) 4815–4822.
[28] Y. Xiao, G. Tian, W. Li, et al., J. Am. Chem. Soc. 141 (2019) 2508–2515.
[29] Y. Xing, X. Wang, S. Hao, et al., Chin. Chem. Lett. 32 (2021) 13–20.
[30] L. Duan, C. Wang, W. Zhang, et al., Chem. Rev. 121 (2021) 14349–14429.
[31] L. Balducci, D. Bianchi, R. Bortolo, et al., Angew. Chem. Int. Ed. 42 (2003) 4937–4940.
[32] Y. Gu, Q. Li, D. Zang, et al., Angew. Chem. Int. Ed. 60 (2021) 13310–13316.
[33] G. Tanarungsun, W. Kiatkittipong, P. Praserthdam, et al., Chemistry 14 (2008) 596–601.
[34] J. Li, Y. Xu, Z. Ding, et al., Chem. Eng. J. 388 (2020) 124248.
[35] X. Shi, S. Liu, C. Duanmu, et al., Chem. Eng. J. 420 (2021) 129976.
[36] J.H. Yang, S. G, Y.J. Gao, et al., Energy Environ. Sci. 6 (2013) 793–798.
[37] H. Zhou, Y. Zhao, J. Gan, et al., J. Am. Chem. Soc. 142 (2020) 12643–12650.
[38] Y. Zhong, G. Li, L. Zhu, et al., J. Mol. Catal. A: Chem. 272 (2007) 169–173.
[39] Y. Zhang, S.J. Park, J. Catal. 379 (2019) 154–163.
[40] Y. Pan, Y. Chen, K. Wu, et al., Nat. Commun. 10 (2019) 4290.
[41] Z. Wei, F.A. Villamena, L.K. Weavers, Environ. Sci. Technol. 51 (2017) 3410–3417.